energies

MDPI

Article

A Fast DC Fault Detection Method for Multi-Terminal AC/DC Hybrid Distribution Network Based on Voltage Change Rate of DC Current-Limiting Inductor

Xiaomin Qi [1,2,*], Wei Pei [1,2], Luyang Li [1,2] and Li Kong [1,2]

1 Institute of Electrical Engineering, Chinese Academy of Sciences, Beijing 100190, China; peiwei@mail.iee.ac.cn (W.P.); liluyang@mail.iee.ac.cn (L.L.); kongli@mail.iee.ac.cn (L.K.)
2 School of Electronic, Electrical and Communication Engineering, University of Chinese Academy of Sciences, Beijing 100049, China
* Correspondence: xiaomin.qi@mail.iee.ac.cn; Tel.: +86-152-0134-2735

Received: 12 June 2018; Accepted: 9 July 2018; Published: 12 July 2018

Abstract: The rapid detection of direct current (DC) faults is one of the key technologies for the development of multi-terminal alternating current (AC)/DC hybrid distribution networks. The DC fault current rises quickly and affects the whole network. Therefore, DC faults must be detected much faster than AC faults. This paper proposes a fast DC fault detection method based on the voltage change rate of the current-limiting inductor (CLI) for the multi-terminal AC/DC hybrid distribution network. Firstly, the characteristics of the fault voltages and currents and of the CLIs are studied in detail, and the feasibility of using the voltage change rate of the CLI to detect DC fault is analyzed. Based on this, a primary fault detection method is proposed to identify the faulty line, determine the fault type and the fault poles using the amplitudes of the single-ended CLI voltage change rates. For high-resistance DC faults, a backup detection method using the directions and amplitudes of the voltage change rates of the double-ended CLIs is proposed. Finally, the proposed method is verified by MATLAB simulations. The simulation results show that the proposed method can detect all DC faults accurately, and the faulty line, fault type and fault poles can be determined quickly. The proposed method is not affected by the fault location, current-limiting inductance, power reversal of the converters, AC fault and communication delay.

Keywords: AC/DC hybrid distribution network; DC fault; high-resistance fault; voltage change rate of CLI; fault detection

1. Introduction

In recent years, DC distribution networks and AC/DC hybrid distribution networks are attracting increasing attention due to the increasing demand for distributed generation and the need for regional grid interconnection [1,2]. The AC/DC hybrid distribution network can satisfy the above requirements and achieve the interconnection and transition between the AC distribution network and the DC distribution network. Several AC distribution networks can be connected through DC lines, which can form a DC distribution network. Then, the entire AC and DC network can be called a regional multi-terminal AC/DC hybrid distribution network [3]. Due to the low impedance of the DC distribution network, the fault currents will increase rapidly after a DC fault [4]. More seriously, in the multi-terminal AC/DC hybrid distribution network, the fault currents of different converters are superimposed over each other, which results in the higher demands on the semiconductor devices in the system. If the fault cannot be detected as soon as possible and the faulty line is not isolated timely,

the entire system will withstand significant losses. Therefore, it is necessary to carry out research on the fast detection method of DC faults in a multi-terminal AC/DC hybrid distribution network.

The research of the DC fault detection methods usually includes the primary detection methods and the backup detection methods. The primary detection methods mainly focus on the faults with low resistances, and the backup detection methods are mainly for the high-resistance faults. The fault currents of low-resistance faults are higher than that of high-resistance faults, which has a strict requirement for fault detection speed. It must be detected within 2 ms after the fault [5]. Meanwhile the fault currents of high-impedance faults are lower, and the requirement for fault detection speed is relatively easier to meet. However, the backup detection method needs to detect all high-resistance faults accurately that are beyond the detection scope of the primary detection method.

References [6,7] use the current difference between the two ends of the DC line to identify the DC faulty line. This method requires the communication between both ends and is vulnerable to communication delay. The fault detection speed is low. Reference [8] uses the first-order differential and second-order differential of the fault current to detect DC faults in a multi-terminal system, but this method is only useful for fault resistances below 10 Ω. As the fault resistance increases, the differential of the fault current will decrease, and false detection may occur. A voltage change rate-based fault detection method is proposed in [9,10], but it can only identify the faulty line and the fault type and fault poles are unknown. Reference [11] uses the ratios of the high-frequency transient voltage amplitudes at the two ends of the CLI to detect DC faults. In addition, reference [12] uses the ratios of the high-frequency transient voltage and current of the CLI to identify the fault type. However, the high-frequency transient signals can be affected by noise sometimes.

For the detection of high-resistance faults, a method based on the magnitude of the voltage change rate of the DC line is proposed in [13]. While the fault type and fault poles cannot be identified by this method. In ref. [14], a passive oscillation circuit is used to detect the DC high-resistance fault. The capacitors are connected to the CLIs in parallel to form the LC resonant circuits. The faults are identified by detecting the current components at a specific frequency after the faults. However, these components will decrease with the increase of the fault resistance. Therefore, it will be difficult to detect the fault when the fault resistance is high. When the detection of the DC fault is completed by the fault detection devices, the signal will be sent to the protection devices such as the DC circuit breakers and so on. Subsequently, the DC fault will be isolated quickly and successfully [15–18].

Research has also been carried out on the protection scheme of the DC grid [19–26]. A system protection scheme for the low-voltage DC microgrid is proposed in reference [22]. However, this method mainly aims at the design of the protection scheme and the selection of the protection devices. Reference [23] proposes an overcurrent-based DC distribution network protection scheme, which also focuses on the design of protection schemes. Based on the detailed analysis of the DC fault characteristics of the DC grid, reference [24] summarizes the short-comings of the existing unit protection and non-unit protection methods. Then a flexible protection scheme design framework is proposed. Reference [25] proposes a protection scheme focusing on the control for the short-circuit current and the fault ride-through scheme for the low-voltage distribution network. Reference [26] focuses on the design of the electrical protection system of the multiterminal DC compact node. However, all the above studies focus on the protection scheme design for the DC faults. As the basis of the design of the protection scheme, the fault detection method is not investigated thoroughly.

In summary, research on DC fault detection methods for multi-terminal systems are still not comprehensive and in-depth. Therefore, it is urgent to design a fast detection method for DC faults that can identify the faulty line, determine the fault type and the fault poles quickly and accurately for multi-terminal AC/DC hybrid distribution networks.

Based on existing research, the voltage and current characteristics of CLIs after DC faults are analyzed in detail for a multi-terminal AC/DC hybrid distribution network in this paper. Then a DC fault detection method based on the voltage change rates of the CLIs is proposed. The method consists

of two parts: a primary detection method and a backup detection method. The primary detection method uses the amplitude of the single-ended CLI voltage change rate to identify the faulty line, determine the fault type and the fault poles. The detection is fast and accurate. The backup detection method achieves the detection of the high-resistance faults by comparing the directions and amplitudes of the voltage change rates of the CLIs at both ends of the DC lines. Finally, the feasibility of the proposed method under different fault resistances, fault locations and current-limiting inductances is verified by simulations. In addition, the simulation results show that the proposed method is not affected by the power reversal of the converters, AC fault and communication delay.

2. Analysis of Fault Characteristics of CLI Voltage and Current

This section takes the multi-terminal radial AC-DC hybrid distribution network as an example to study. It is known from [27] that after a DC pole-to-pole fault or a DC pole-to-ground fault, the insulated gate bipolar transistors (IGBTs) of the converters will be blocked immediately. In addition, both faults include the capacitor discharge stage and the AC current feeding stage. To prevent the anti-parallel diodes of the IGBTs from being damaged by the overcurrent at the end of the capacitor discharge stage, the DC circuit breakers need to isolate the faulty line before the end of this stage [28]. Therefore, the fault detection must also be completed before the end of the capacitor discharge stage. Therefore, this paper mainly analyzes the fault characteristics of the CLI voltage and current during the capacitor discharge stage.

When the pole-to-pole fault F1 occurs on the DC line, the voltage source converters (VSCs) can be represented by their DC capacitors. The equivalent circuit of the three-terminal radial AC/DC hybrid distribution network during the capacitor discharge stage is shown in Figure 1.

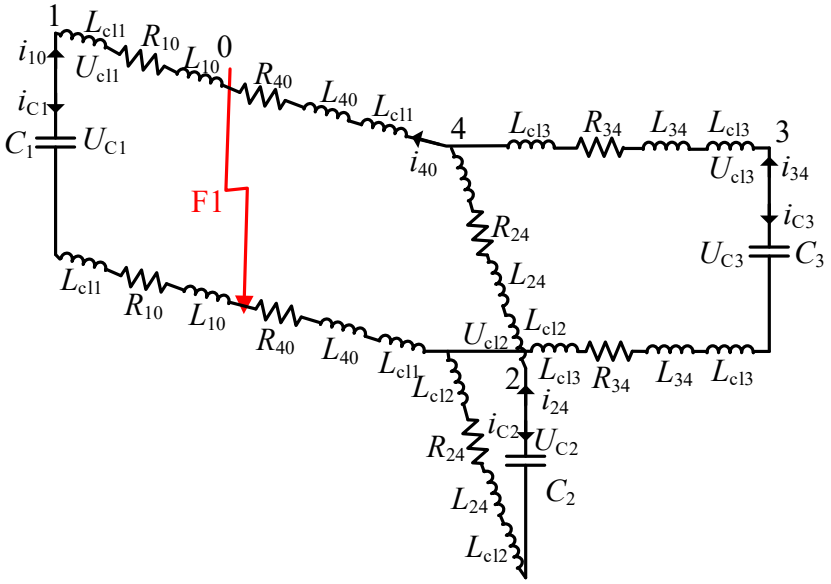

Figure 1. Equivalent circuit for fault F1 of the multi-terminal radial AC/DC hybrid distribution network.

In Figure 1, C_1, C_2 and C_3 are the equivalent DC capacitors of three converters. L_{cl1}, L_{cl2} and L_{cl3} are the inductances of the CLIs. R_{10} and L_{10} are the equivalent resistance and inductance of the DC line between the fault converter and the fault point. R_{40} and L_{40} are the equivalent resistance and inductance of the DC line between the fault point and the common point. R_{24}, L_{24} and R_{34}, L_{34} are the equivalent resistances and inductances of the DC lines of converter 2 and converter 3 respectively. U_{cl1}, U_{cl2} and U_{cl3} are the voltages of the CLIs. U_{C1}, U_{C2} and U_{C3} are the voltages of the DC capacitors. When the pole-to-pole fault F1 occurs on DC line 14, the DC capacitors of all the converters start

to discharge. The converters can be represented by their DC capacitors and the DC lines can be represented by the series of the line resistances and line inductors. Then the faulty line 14 is divided into two parts. One is from the converter 1 to the fault point and the other is from the fault point to the common point. Thus, during the DC capacitor discharge stage, the differential equations for the system can be obtained according to Figure 1 as:

$$\begin{cases} U_{C1} = 2R_{10}i_{10} + 2(L_{10} + L_{cl1})\frac{di_{10}}{dt} + R_f(i_{10} + i_{40}) \\ U_{C2} = 2R_{24}i_{24} + 2(L_{24} + L_{cl2})\frac{di_{24}}{dt} + 2R_{40}i_{40} + 2(L_{40} + L_{cl1})\frac{di_{40}}{dt} \\ U_{C3} = 2R_{34}i_{34} + 2(L_{34} + L_{cl3})\frac{di_{34}}{dt} + 2R_{40}i_{40} + 2(L_{40} + L_{cl1})\frac{di_{40}}{dt} \end{cases} \quad (1)$$

$$\begin{cases} i_{40} = i_{24} + i_{34} \\ i_{10} = -i_{C1} = C_1\frac{dU_{C1}}{dt} \\ i_{24} = -i_{C2} = C_2\frac{dU_{C2}}{dt} \\ i_{34} = -i_{C3} = C_3\frac{dU_{C3}}{dt} \end{cases} \quad (2)$$

Then the currents of the CLIs on DC lines during the capacitor discharge stage can be obtained by solving (1) and (2). The voltage change rates of all CLIs can be expressed as:

$$\begin{cases} \frac{dU_{cl1}}{dt} = L_{cl1}\frac{d^2i_{10}}{dt^2} \\ \frac{dU_{cl2}}{dt} = L_{cl2}\frac{d^2i_{24}}{dt^2} \\ \frac{dU_{cl3}}{dt} = L_{cl3}\frac{d^2i_{34}}{dt^2} \end{cases} \quad (3)$$

As shown in (1), there is coupling between the differential equations of the non-faulty lines. It is difficult to get the analytical solutions of the voltage change rates of CLIs on the non-faulty lines. Equation (1) shows that the difference between the forms of the differential equations for the non-faulty lines and the faulty line is only shown by the third term on the right side. This is caused by the fault currents of non-faulty lines 24 and 34 and the equivalent resistance, inductance, and CLI of line 40, which leads to the coupling between the lines 24 and 34. However, the coupling only results in the difference of the magnitudes and directions of the voltage change rates of the CLIs between the faulty line and the non-faulty lines. The characteristics of the voltage change rates of the CLIs on the non-faulty lines are not affected by the coupling. Therefore, the equation of the faulty line is taken as an example here. The fault current of the faulty line can be expressed by solving (1) and (2) as:

$$i_{10} = -\frac{I_{01}\omega_{01}}{\omega_1}e^{-\delta_1 t}\sin(\omega_1 t - \beta_1) + \frac{U_{01}}{\omega_1 L_1}e^{-\delta_1 t}\sin\omega_1 t \quad (4)$$

where U_{01} is the initial value of the DC capacitor voltage. I_{01} is the initial value of the line current. $\delta_1 = R_{10}/L_1$, ${\omega_1}^2 = 1/L_1C_1 - \delta_1^2$, $L_1 = 2(L_{10} + L_{cl1})$, $\omega_{01}^2 = \delta_1^2 + \omega_1^2$, $\beta_1 = \arctan(\omega_1/\delta_1)$.

Substituting (4) into (3) yields:

$$\frac{dU_{cl1}}{dt} = L_{cl1}e^{-\delta_1 t}[-\frac{I_{01}\omega_{01}^3}{\omega_1}\sin(\omega_1 t - 3\beta_1) + \frac{U_{01}\omega_{01}^2}{\omega_1 L_1}\sin(\omega_1 t - 2\beta_1)] \quad (5)$$

When $t = 0$, the voltage change rate of L_{cl1} is:

$$\frac{dU_{cl1}}{dt}(t=0) = L_{cl1}[I_{01}(4\delta_1^2 - \omega_{01}^2) - \frac{2U_{01}\delta_1}{L_1}] \quad (6)$$

As shown in (4)–(6), the current of the CLI on the faulty line increases rapidly after the DC pole-to-pole fault. In addition, the CLI voltage rises at the same time from a value close to 0. Therefore, at the moment of the fault occurrence, the voltage change rate of the CLI on the faulty line will increase immediately. The CLI voltage and current will attenuate gradually afterwards, and the voltage change

rate also decreases. For non-faulty lines, it can be seen from (1) that the CLI voltages and currents have similar characteristics except that the amplitudes and directions are different.

For the pole-to-ground fault, the impedance of the faulty line circuit during the capacitor discharge stage is only half of that of the pole-to-pole fault. Therefore, the voltage and current characteristics of the CLI are similar to the above analysis. After a pole-to-ground fault, the voltage change rate of the CLI on the faulty line can be expressed as:

$$\frac{\mathrm{d}U_{\mathrm{cl1}}}{\mathrm{d}t} = -C_1 L_{\mathrm{cl1}}(A\lambda_1^3 e^{\lambda_1 \mathrm{t}} + B\lambda_2^3 e^{\lambda_2 \mathrm{t}}) \tag{7}$$

$$\begin{cases} \lambda_{1,2} = -\frac{R_2}{2L_2} \pm \sqrt{(\frac{R_2}{2L_2})^2 - \frac{1}{2L_2C_1}} \\ A = \frac{1}{\lambda_1 - \lambda_2}(-\frac{I_{01}}{C_1} - U_{01}\lambda_2) \\ B = \frac{1}{\lambda_1 - \lambda_2}(\frac{I_{01}}{C_1} + U_{01}\lambda_1) \end{cases} \tag{8}$$

where, $R_2 = R_{10} + R_{\mathrm{f}}$, $L_2 = L_{10} + L_{\mathrm{cl1}}$. When $t = 0$, the voltage change rate of the CLI on the faulty line is:

$$\frac{\mathrm{d}U_{\mathrm{cl1}}}{\mathrm{d}t}(t=0) = L_{\mathrm{cl1}}[I_{01}(\frac{2R_2^2}{L_2^2} - \frac{1}{L_2C_1}) - \frac{U_{01}R_2}{L_2^2}] \tag{9}$$

As shown in (7)–(9), after the pole-to-ground fault, the voltage change rate of the CLI on the faulty line reaches a maximum value quickly and then attenuates gradually, which is similar to that of the pole-to-pole fault. The simulation results of the currents and voltages of the CLIs during the pole-to-pole fault and pole-to-ground fault are shown in Figure 2.

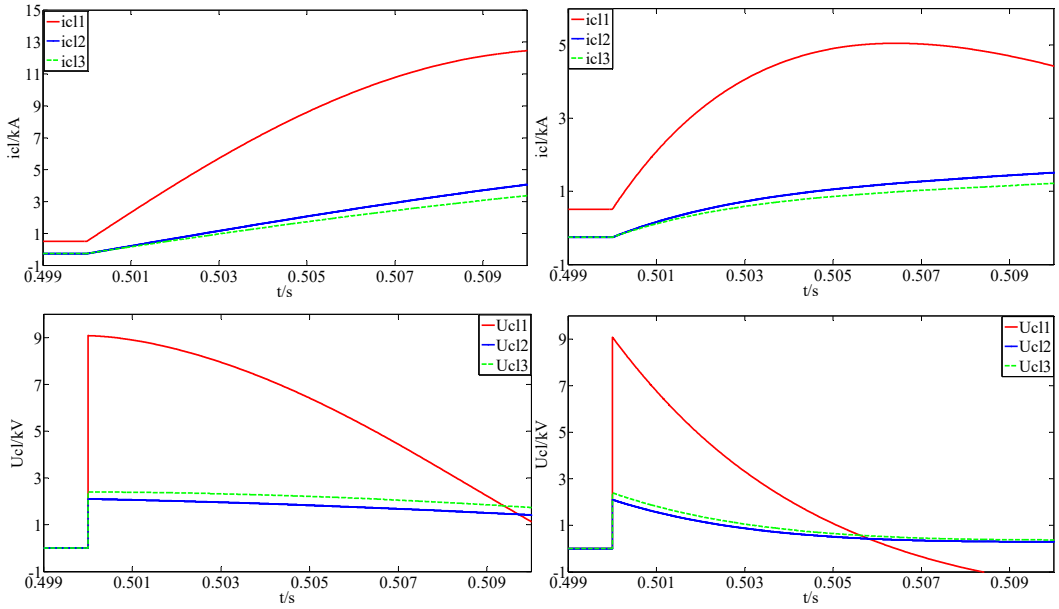

(a) Pole-to-pole fault (b) Pole-to-ground fault

Figure 2. Simulation results of the currents and voltages of the CLIs during DC faults in the multi-terminal radial AC/DC hybrid distribution network.

As shown in Figure 2, after a DC fault, the rapid rise of the fault current causes the CLI voltages increasing to a peak value in a short time and then attenuating gradually with the decrease of the current change rates of the CLIs. The voltages of the CLIs are close to 0 during the normal operation. Therefore, the magnitudes of the CLI voltage change rates can be used to achieve fast and accurate detection of the DC faults. In addition, for the pole-to-pole fault and the pole-to-ground fault, the voltage change rate of the CLI on the faulty line is much higher than those on the non-faulty

lines. Therefore, the faulty line identification, fault type determination and fault poles identification can be realized by comparing the voltage change rates of CLIs on different lines. Based on the above analysis, we can conclude that the voltage change rates of the CLIs can be used to detect the DC faults in a multi-terminal AC/DC hybrid distribution network.

3. Primary Fault Detection Method

This paper proposes a method for the fast detection of DC faults in a multi-terminal AC/DC hybrid distribution network based on the voltage change rates of the CLIs. The method includes a primary detection method and a backup detection method. The primary detection method is for usual low-resistance faults and the backup detection method is for high-resistance faults. This section gives a detailed introduction and analysis of the primary detection method.

The primary detection method includes three parts: faulty line identification, fault type determination, and fault poles identification.

3.1. Faulty Line Identification

From the analysis of the first section of this paper, we can see that after a DC fault, the faulty lines can be identified by detecting whether the voltage change rate of the CLI on each line is higher than the given threshold. The faulty line identification criterion is:

$$\left|\frac{\mathrm{d}U_{\mathrm{cli}}}{\mathrm{d}t}\right| > \frac{\mathrm{d}U_{\mathrm{thl}}}{\mathrm{d}t} \tag{10}$$

where, i is the number of the CLIs, $\mathrm{d}U_{\mathrm{thl}}/\mathrm{d}t$ is the faulty line identification threshold, which can be selected by the calculation and simulation. When the voltage change rate of CLI on a certain line satisfies (10), it can be determined that this line is the faulty line.

3.2. Fault Type Determination

The fault type determination means the judgment of the pole-to-pole fault and the pole-to-ground fault. During a pole-to-pole fault, the positive-pole and negative-pole CLIs are both in the capacitor discharge circuit. Therefore, the voltage change rates of the positive-pole and negative-pole CLIs are almost equal. However, for the pole-to-ground fault, the voltage change rates of the positive-pole and negative-pole CLIs are completely different. This characteristic can be used as the determination criteria of the fault type:

$$\begin{cases} \left|\left|\frac{\mathrm{d}U_{\mathrm{clip}}}{\mathrm{d}t}\right| - \left|\frac{\mathrm{d}U_{\mathrm{clin}}}{\mathrm{d}t}\right|\right| < \left|\frac{\mathrm{d}U_{\mathrm{tht}}}{\mathrm{d}t}\right|, \text{pole-to-pole fault} \\ \left|\left|\frac{dU_{\mathrm{clip}}}{\mathrm{d}t}\right| - \left|\frac{\mathrm{d}U_{\mathrm{clin}}}{\mathrm{d}t}\right|\right| \geq \left|\frac{\mathrm{d}U_{\mathrm{tht}}}{\mathrm{d}t}\right|, \text{pole-to-ground fault} \end{cases} \tag{11}$$

where, U_{clip} and U_{clin} are the voltages of the positive-pole and negative-pole CLIs respectively. $\mathrm{d}U_{\mathrm{tht}}/\mathrm{d}t$ is the fault type determination threshold. When the absolute value of the difference between the voltages of the positive-pole and negative-pole CLIs on the faulty line is lower than the fault type determination threshold, it can be concluded that the fault is a pole-to-pole fault. Otherwise, the fault is a pole-to-ground fault.

3.3. Fault Poles Identification

If in Section 3.2, the fault is determined to be a pole-to-pole fault, there is no need to determine the fault poles. If it is determined that the fault is a pole-to-ground fault, a further identification of the fault pole is required. The proposed fault poles identification criteria are:

$$\begin{cases} \left|\frac{\mathrm{d}U_{\mathrm{clip}}}{\mathrm{d}t}\right| - \left|\frac{\mathrm{d}U_{\mathrm{clin}}}{\mathrm{d}t}\right| > \frac{\mathrm{d}U_{\mathrm{thp}}}{\mathrm{d}t}, \text{positive pole-to-ground fault} \\ \left|\frac{\mathrm{d}U_{\mathrm{clip}}}{\mathrm{d}t}\right| - \left|\frac{\mathrm{d}U_{\mathrm{clin}}}{\mathrm{d}t}\right| < -\frac{\mathrm{d}U_{\mathrm{thp}}}{\mathrm{d}t}, \text{negative pole-to-ground fault} \end{cases} \tag{12}$$

where, $d U_{thp}/dt$ is the fault poles identification threshold. When the difference between the voltage change rates of the positive-pole and negative-pole CLIs is higher than the threshold, the positive-pole is the fault pole. When this difference is negative and less than the threshold, a negative pole-to-ground fault is determined.

The value of the faulty line identification threshold, the fault type determination threshold and the fault poles identification threshold can be defined according to (4)–(9). The voltage change rates of all the CLIs can be obtained by solving (1)–(3). For the faulty line identification threshold, its value should be higher than the maximum value of the voltage change rates of the CLIs on the non-faulty lines and lower than the minimum value of the voltage change rate of the CLI on the faulty line. The higher the faulty line identification threshold is, the more accurate the faulty line identification will be and the longer the time for the identification will be. Therefore, the exact value of the faulty line identification threshold should be defined according to the requirement of the fault detection. For the fault type determination threshold and the fault poles identification threshold, their values can be set to 0 theoretically. However, to provide enough margin, their values should be a little higher than 0. In addition, the maximum values of them are mainly limited by the fault detection time.

The flow chart of the primary fault detection method for DC faults is shown in Figure 3.

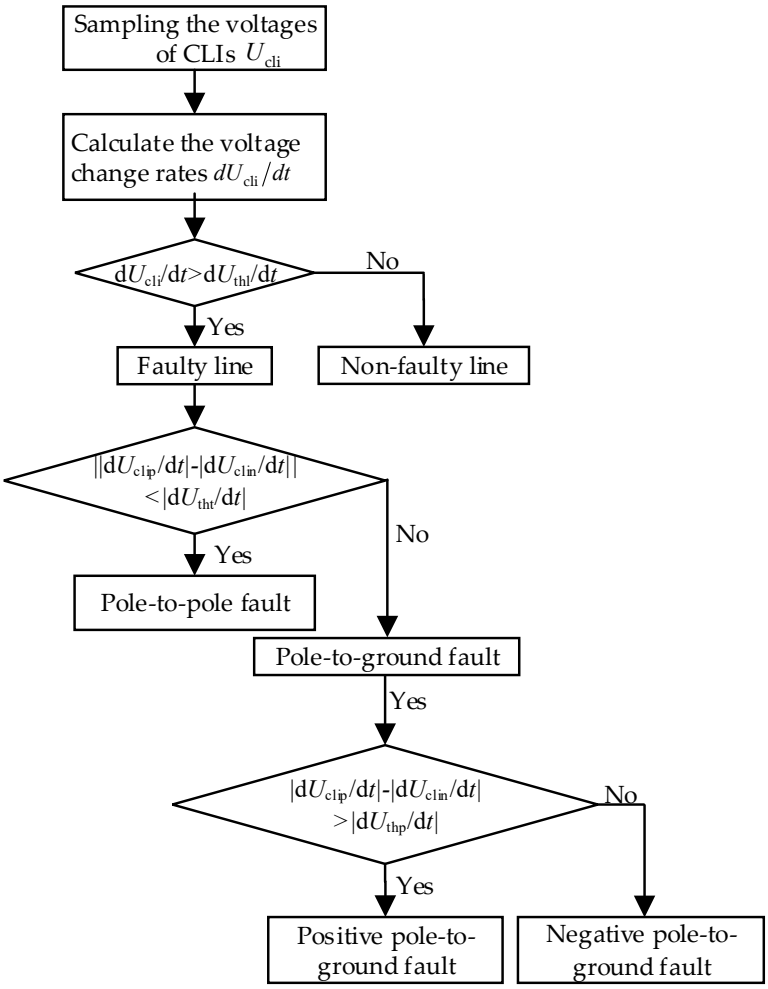

Figure 3. Flow chart of the proposed primary fault detection method for DC faults.

As shown in Figure 3, the first step of the primary fault detection method proposed in this paper is to acquire the voltage signals of the CLIs and calculate the voltage change rates of them. Then according to the criteria of the faulty line identification, fault type discrimination and fault poles

identification, the fault poles can be determined. Finally, the trigger signal is sent to the protection devices of the fault poles.

The proposed method uses only the data of the single-ended CLI to achieve the faulty line identification, fault type determination and fault poles identification. The communication between the two ends of DC lines is unnecessary. Therefore, it is fast and accurate enough for the detection of DC faults.

4. Backup Fault Detection Method

When a high-resistance fault occurs, the voltage change rates of the CLIs are much lower than that of the usual DC faults. The primary fault detection method may fail, and the fault cannot be detected correctly. Therefore, this section proposes a backup fault detection method for the high-resistance faults.

The backup fault detection method includes two parts: faulty line identification and fault type determination. Let the bus-to-line direction be the positive direction. For the faulty line, the directions of the voltage change rates of the CLIs at the two ends are always opposite to each other. While the voltage change rates of the CLIs at the two ends of the non-faulty lines are in the same directions. Therefore, this characteristic can be used to identify the faulty line. The faulty line identification criteria are:

$$\begin{cases} \frac{\mathrm{d}U_{\mathrm{clis}}}{\mathrm{d}t} \cdot \frac{\mathrm{d}U_{\mathrm{clif}}}{\mathrm{d}t} < 0, \text{faulty line} \\ \frac{\mathrm{d}U_{\mathrm{clis}}}{\mathrm{d}t} \cdot \frac{\mathrm{d}U_{\mathrm{clif}}}{\mathrm{d}t} > 0, \text{non-faulty line} \end{cases} \tag{13}$$

where, $\mathrm{d}U_{\mathrm{clis}}/\mathrm{d}t$ and $\mathrm{d}U_{\mathrm{clif}}/\mathrm{d}t$ are the voltage change rates of the CLIs on two ends of the DC lines respectively. The faulty line of the high-resistance fault can be identified according to (13). This method is not affected by the fault resistance and is suitable for the high-resistance fault.

According to the analysis of the second section of this paper, after a pole-to-pole fault, the voltage change rates of the positive pole and negative pole CLIs are almost the same. While for the pole-to-ground fault, the voltage change rates of the positive-pole and negative-pole CLIs are completely different. Therefore, the fault type can be determined based on the following criteria:

$$\begin{cases} \left|\frac{\mathrm{d}U_{\mathrm{clip}}}{\mathrm{d}t}\right| - \left|\frac{\mathrm{d}U_{\mathrm{clin}}}{\mathrm{d}t}\right| > \frac{\mathrm{d}U_{\mathrm{thb}}}{\mathrm{d}t}, \text{positive pole-to-ground fault} \\ \left|\frac{\mathrm{d}U_{\mathrm{clip}}}{\mathrm{d}t}\right| - \left|\frac{\mathrm{d}U_{\mathrm{clin}}}{\mathrm{d}t}\right| < -\frac{\mathrm{d}U_{\mathrm{thb}}}{\mathrm{d}t}, \text{negative pole-to-ground fault} \\ -\frac{\mathrm{d}U_{\mathrm{thb}}}{\mathrm{d}t} \le \left|\frac{\mathrm{d}U_{\mathrm{clip}}}{\mathrm{d}t}\right| - \left|\frac{\mathrm{d}U_{\mathrm{clin}}}{\mathrm{d}t}\right| \le \frac{\mathrm{d}U_{\mathrm{thb}}}{\mathrm{d}t}, \text{pole-to-pole fault} \end{cases} \tag{14}$$

where, $\mathrm{d}U_{\mathrm{thb}}/\mathrm{d}t$ is the fault type identification threshold. When the voltage change rates of the CLIs at the two ends of the faulty line satisfies (14), the fault type of the high-resistance fault can be determined. The value of the faulty fault type identification threshold can be set to 0 theoretically. However, to provide enough margin and selectivity, its value can be higher than 0. In addition, the maximum value is mainly determined by the requirement of the fault detection time.

The flow chart of the proposed backup fault detection method is shown in Figure 4.

As shown in Figure 4, the voltage change rates of the CLIs at both ends of the DC lines are compared in the backup fault detection method. Therefore, the detection time is longer than that of the primary detection method. However, the fault current of the high-resistance fault is much smaller than that of the usual fault, which leads to a lower requirement for the detection time. In addition, the proposed method only needs to send the fault detection signals at one end to the other, so the fault detection result is not affected by the communication delay.

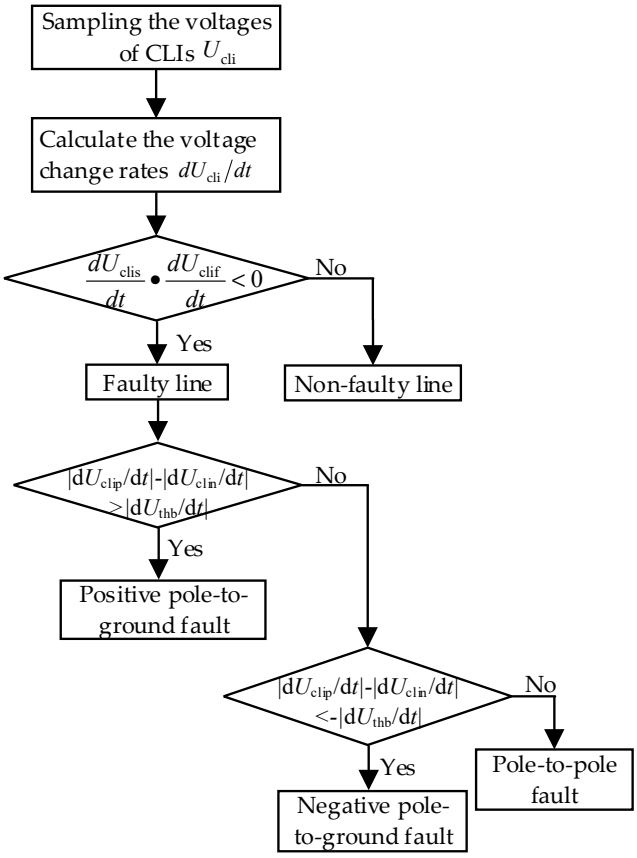

Figure 4. Flow chart of the proposed backup fault detection method for DC faults.

5. Simulation

Figure 5 shows the simulation model of the three-terminal radial AC-DC hybrid distribution network built in MATLAB. Converter 1 uses the constant DC voltage control. Converters 2 and 3 use the constant active power control. The parameters of the simulation model are shown in Table 1.

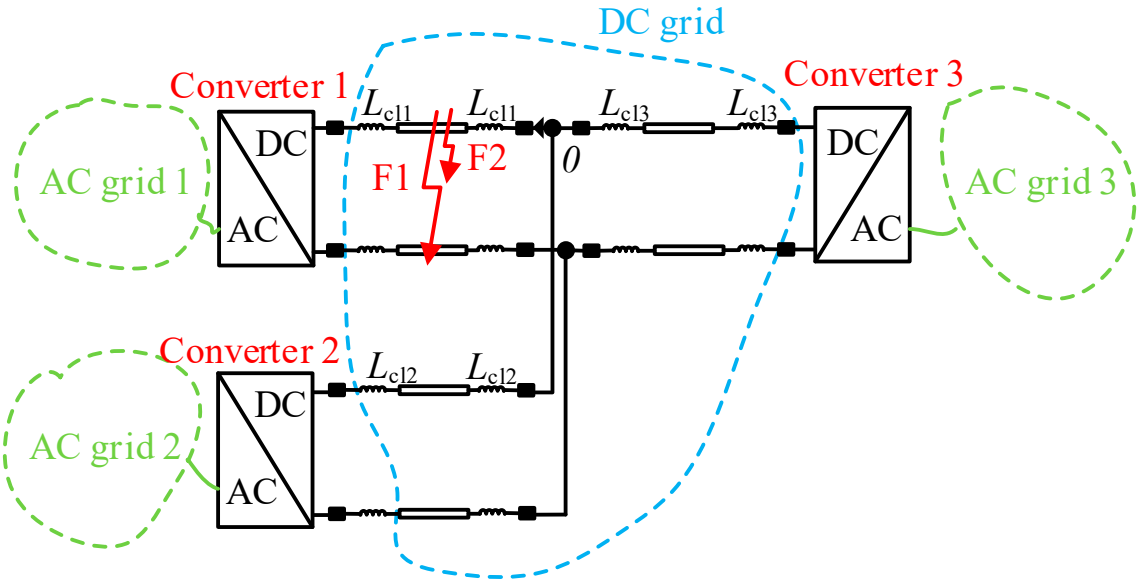

Figure 5. Simulation model of multi-terminal radial AC/DC hybrid distribution network.

Table 1. Parameters of the simulation model.

Parameter	Value	Parameter	Value
DC voltage	20 kV	Line resistance	0.121 Ω/km
Power of converter 1	5 MW	Line inductance	0.97 mH/km
Power of converter 2	−2.5 MW	Power of converter 3	−2.5 MW
L_{cl1}, L_{cl2} and L_{cl3}	5 mH	DC capacitor	4800 mH/km

The simulation model consists of three AC distribution networks which are connected by DC distribution network. The DC circuit breakers and CLIs are configured at both ends of each DC line.

5.1. Primary Detection Method Verification

The pole-to-pole fault and pole-to-ground fault are applied at 0.5 s at the fault positions F1 and F2 respectively. In addition, the voltages of the CLIs during the faults are shown in Figure 6.

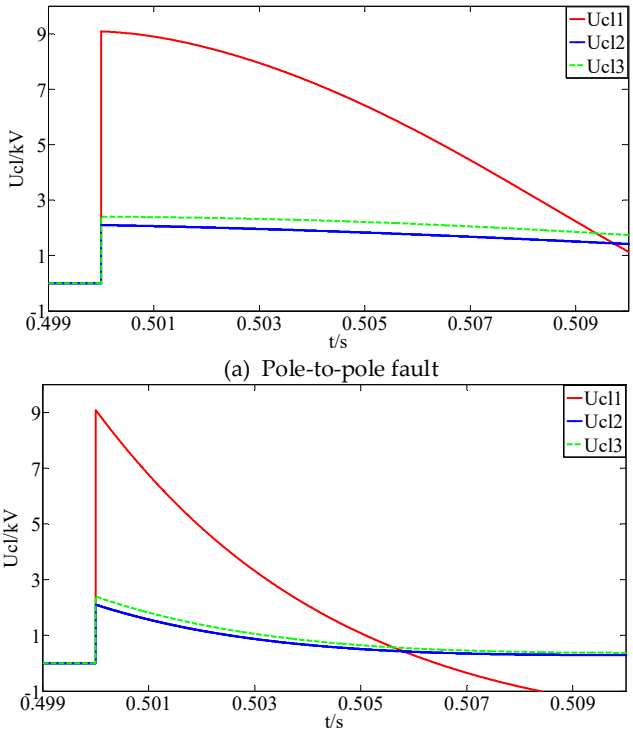

(a) Pole-to-pole fault

(b) Pole-to-ground fault

Figure 6. Simulation results of the voltages of the CLIs during DC faults.

As shown in Figure 6, after the DC faults F1 and F2, the currents flowing through the CLIs on all DC lines increase rapidly, which cause the voltages to increase immediately from 0 during normal operations. Then the voltages of the CLIs attenuate gradually, which is consistent with the above analysis. There is an evident difference in the voltage change rates of the CLIs on the faulty and non-faulty lines.

The pole-to-pole fault and pole-to-ground fault are detected using the proposed primary detection method. According to the system parameters, the faulty line identification threshold, fault type determination threshold and fault poles identification threshold are set at 5.924×10^7 kV/ms, 1×10^7 kV/ms and 4.7×10^7 kV/ms respectively. The fault detection results of the pole-to-pole and pole-to-ground faults are shown in Table 2.

Table 2. Detection results of DC faults.

Fault Resistance (Ω)	Fault Criteria (kV/ms)				
	DC Line	Faulty Line	Fault Type	Fault Poles	Detection Results
0.001	10	1.8126×10^8	0	0	10 pole-to-pole
	20	4.8063×10^7			
	30	4.2395×10^7			
1	10	1.7895×10^8	1.7853×10^8	1.7853×10^8	10 positive pole-to-ground
	20	4.7453×10^7			
	30	4.1859×10^7			

Table 2 shows that after the pole-to-pole and pole-to-ground faults, the voltage change rates of the CLIs on the faulty lines are higher than the faulty line identification threshold 5.924×10^7 kV/ms. In addition, the voltage change rates of the CLIs on the non-faulty lines are less than 5.924×10^7 kV/ms. The faulty lines can be identified correctly. For the pole-to-pole fault, the difference between voltage change rates of the positive pole and negative pole CLIs on the faulty line is 0, which is lower than the fault type determination threshold 1×10^7 kV/ms. Therefore, the pole-to-pole fault can be determined accurately. For the pole-to-ground fault, the fault type determination difference is higher than 1×10^7 kV/ms, so the fault type can be correctly identified. This difference satisfies the fault poles identification criteria at the same time. Therefore, it is determined to be a positive pole-to-ground fault.

Above all, the proposed primary fault detection method can achieve fast and accurate detection of the DC faults in the multi-terminal radial AC/DC hybrid distribution network.

5.2. Backup Detection Method Verification

The pole-to-pole fault and pole-to-ground fault are applied at 0.5 s at the fault positions F1 and F2 respectively. In addition, the fault resistance varies from 0 Ω to 80 Ω. The voltage change rates of the CLIs are shown in Figure 7.

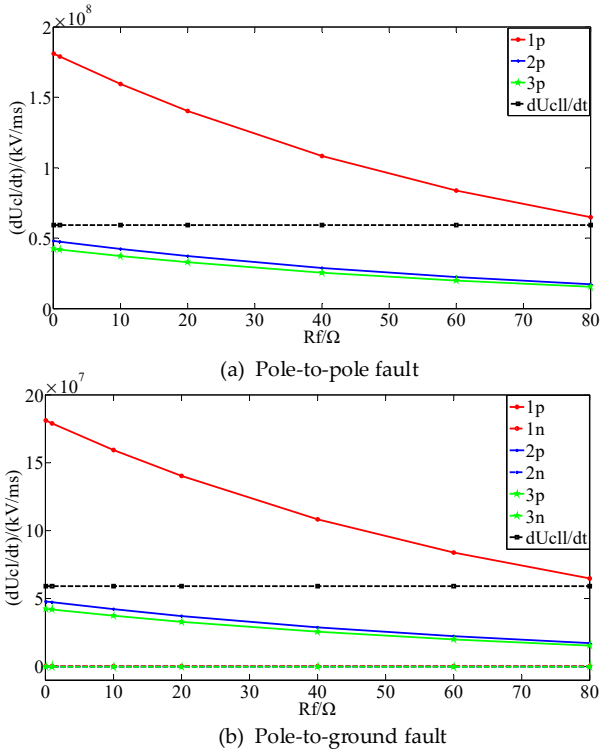

Figure 7. Voltage change rates of the CLIs during DC faults with different fault resistances.

As shown in Figure 7, as the fault resistance increases, the voltage change rates of the CLIs decrease. This is because the increase in the fault resistance leads to the increase of the impedances of the capacitor discharge circuits, which results in a reduction in the rise rates of the fault currents and a decrease in the voltage change rates of the CLIs. When the fault resistance is less than 80 Ω, the voltage change rates of the CLIs on the faulty line and the non-faulty lines are always higher than the faulty line identification threshold 5.924×10^7 kV/ms, so the primary fault detection method can achieve fault detection correctly. The fault detection results when the fault resistance varies are shown in Table 3.

Table 3. Detection results of different fault resistances.

Fault Resistance/Ω	Fault Criteria (kV/ms)				
	DC Line	Faulty Line	Fault Type	Fault Poles	Detection Results
0.1	10	1.8103×10^8	0	0	10 pole-to-pole
	20	4.8002×10^7			
	30	4.2341×10^7			
1	10	1.7895×10^8	1.7853×10^8	1.7853×10^8	10 positive pole-to-ground
	20	4.7453×10^7			
	30	4.1859×10^7			
10	10	1.5941×10^8	0	0	10 pole-to-pole
	20	4.2297×10^7			
	30	3.7333×10^7			
20	10	1.4019×10^8	1.3977×10^8	1.3977×10^8	10 positive pole-to-ground
	20	3.7224×10^7			
	30	3.2880×10^7			
40	10	1.0840×10^8	0	0	10 pole-to-pole
	20	2.8835×10^7			
	30	2.5516×10^7			
60	10	8.3808×10^7	8.3392×10^7	8.3392×10^7	10 positive pole-to-ground
	20	2.2341×10^7			
	30	1.9819×10^7			
80	10	6.4765×10^7	0	0	10 pole-to-pole
	20	1.7318×10^7			
	30	1.5407×10^7			

As shown in Table 3, when the fault resistance varies, the proposed fault detection method can achieve the faulty line identification, fault type determination, and fault poles identification accurately.

However, obviously, when the fault resistance continues to increase, the voltage change rates of the CLIs will keep decreasing and the voltage change rate of the CLI on faulty line may be lower than the faulty line identification threshold. The primary fault detection method will become ineffective. At the same time, the fault type determination and fault poles identification criteria will also fail. Therefore, when a high-resistance fault occurs in the system, a backup fault detection method needs to be started.

With a fault resistance of 200 Ω, a pole-to-pole fault is applied at the system. The voltages of the CLIs are shown in Figure 8. U_{clips} and U_{clipf} are the voltages of the CLI at the near end and far end of each DC line respectively.

As shown in Figure 8, when the fault resistance is 200 Ω, the directions of the voltage change rates of the CLI at the two ends of the faulty line is different. While for the non-faulty lines, the directions of voltage change rates of the CLIs at two ends are the same. Therefore, the criteria of the backup fault detection method are satisfied, and the faulty line can be identified. When a pole-to-ground fault occurs, the characteristics of the voltage change rates of the CLIs also satisfy the above criteria. The simulation results of the voltage change rates of the positive-pole and negative-pole CLIs at the two ends of the faulty line after the pole-to-pole and pole-to-ground faults are shown in Table 4.

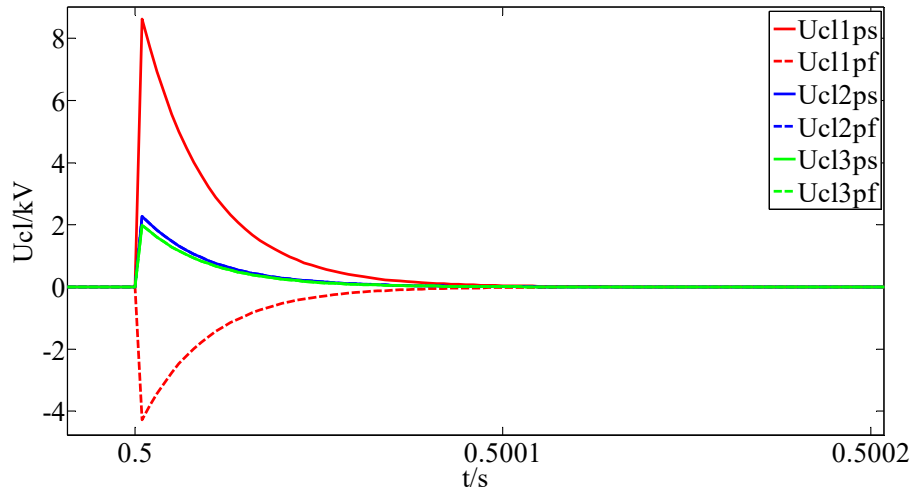

Figure 8. Simulation results of the CLI voltages during a high-resistance pole-to-pole fault.

Table 4. Voltage change rates of the CLIs during a high-resistance DC fault.

Fault Type	DC Line		Voltage Change Rates of CLIs (kV/ms)	
			Near End	Far End
Pole-to-pole fault	10	Positive pole	1.3580×10^7	-7.3593×10^6
		Negative pole	-1.3580×10^7	7.3593×10^6
	20	Positive pole	3.8083×10^6	3.8083×10^6
		Negative pole	-3.8083×10^6	-3.8083×10^6
	30	Positive pole	3.5510×10^6	3.5510×10^6
		Negative pole	-3.5510×10^6	-3.5510×10^6
Pole-to-ground fault	10	Positive pole	1.3583×10^7	-7.3607×10^6
		Negative pole	4.1812×10^5	4.2248×10^5
	20	Positive pole	3.8090×10^6	3.8090×10^6
		Negative pole	-1.0943×10^5	-1.0934×10^5
	30	Positive pole	3.5517×10^6	3.5517×10^6
		Negative pole	-3.1314×10^5	-3.1314×10^5

As shown in Table 4, after the pole-to-pole and pole-to-ground faults, the directions of the voltage change rates of the CLIs at the two ends of the faulty line are different and for the non-faulty line, the two directions are the same, which has been analyzed above. According to the simulation results, the fault type determination threshold is set at 1×10^6 kV/ms. For the pole-to-pole fault, the difference between the voltage change rates of the two poles of the faulty line is close to 0, which is lower than the fault type determination threshold 1×10^6 kV/ms. According to (14), the fault can be identified as a pole-to-pole fault. For the pole-to-ground fault, the difference between the voltage change rates of the two poles of the faulty line is 1.3165×10^7 kV/ms, which is higher than 1×10^6 kV/ms. According to the first equation of (14), the fault can be identified as a pole-to-ground fault.

Above all, the proposed backup fault detection method can achieve accurate detection of the high-resistance faults and make up the weaknesses of the primary detection method. Although the backup detection method requires the communication between both ends of the lines, only the directions and amplitudes of the voltage change rates of the CLIs are sent and the time synchronization is not required at both ends. Therefore, the detection results are not affected by the communication delay, which ensures a great performance.

5.3. Influence of Fault Location on Proposed Method

The pole-to-pole fault and pole-to-ground fault are applied at the system respectively. In addition, the fault distance varies from 0.1 km to 0.99 km. The voltage change rates of the CLIs during the faults are shown in Figure 9.

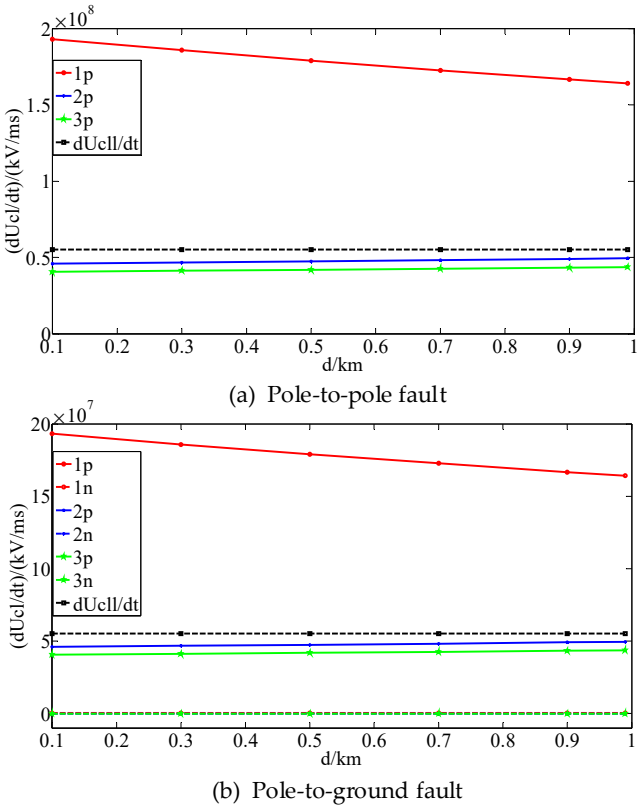

Figure 9. The Influence of Fault Location on the Voltage Change Rates of the CLIs.

Figure 9 shows that as the fault distance increases, the impedance of the capacitor discharge circuit of each converter increases. Therefore, the fault current of each line decreases and the voltage change rates of the CLIs decrease. However, because the DC lines of the AC/DC hybrid distribution network are relatively short, and the line resistances and inductances are both low, the influence of the change in fault location on the voltage change rates of the CLIs is slight. When the fault distance increases gradually, the voltage change rate of the CLI on the faulty line decreases at the same time, and for the non-faulty lines, the rates remain almost constant. The fault detection results when the fault distance varies are shown in Table 5.

Table 5. Detection results of different fault locations.

Fault Distance/km	Fault Criteria (kV/ms)				
	DC Line	Faulty Line	Fault Type	Fault Poles	Detection Results
0.1	10	1.9306×10^8	0	0	10 pole-to-pole
	20	4.5931×10^7			
	30	4.0524×10^7			
0.3	10	1.8574×10^8	1.8532×10^8	1.8532×10^8	10 positive pole-to-ground
	20	4.6681×10^7			
	30	4.1177×10^7			

Table 5. *Cont.*

Fault Distance/km	Fault Criteria (kV/ms)				
	DC Line	Faulty Line	Fault Type	Fault Poles	Detection Results
0.5	10	1.7895×10^8	0	0	10 pole-to-pole
	20	4.7453×10^7			
	30	4.1859×10^7			
0.7	10	1.7261×10^8	1.7219×10^8	1.7219×10^8	10 positive pole-to-ground
	20	4.8254×10^7			
	30	4.2562×10^7			
0.9	10	1.6669×10^8	0	0	10 pole-to-pole
	20	4.9082×10^7			
	30	4.3288×10^7			
0.99	10	1.6416×10^8	0	0	10 pole-to-pole
	20	4.9464×10^7			
	30	4.3624×10^7			

As shown in Table 5, when the fault location varies, the proposed fault detection method can achieve the faulty line identification, fault type determination, and fault poles identification accurately. The fault detection method has high speed and enough accuracy.

5.4. Influence of Current-Limiting Inductance on Proposed Method

The pole-to-pole fault and pole-to-ground fault are applied at the system respectively. In addition, the current-limiting inductance varies from 1 mH to 10 mH. The voltage change rates of the CLIs during the faults are shown in Figure 10.

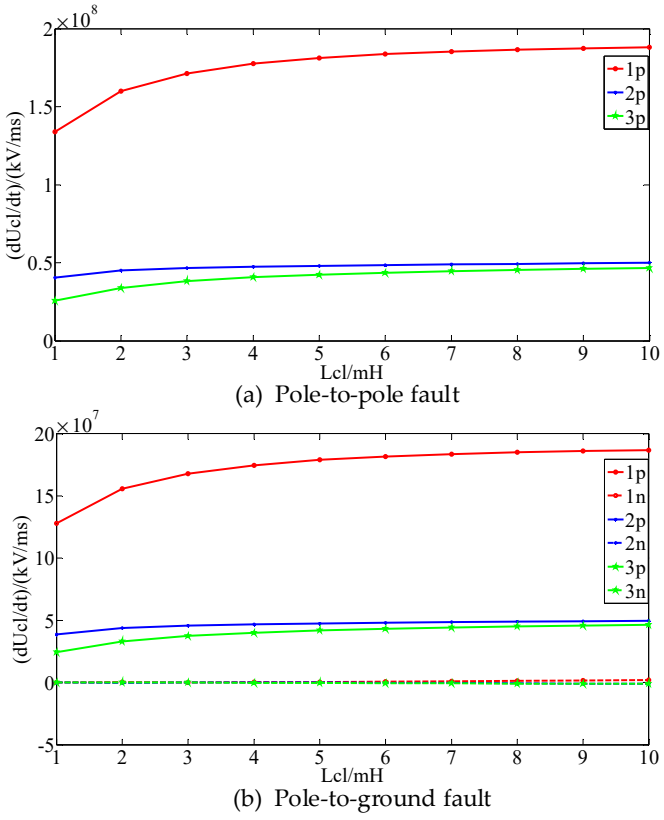

Figure 10. The influence of current-limiting inductance on the voltage change rates of the CLIs.

As shown in Figure 10, for the pole-to-pole and pole-to-ground faults, with the increase of the current-limiting inductances, the voltage change rates of the CLIs on the faulty line and non-faulty lines increase greatly at first and then rise slowly. The voltage change rates of the CLIs on the faulty line is always higher than the faulty line identification threshold. For non-faulty lines, the values are lower than the threshold. The difference of the voltage change rates between the positive-pole and negative-pole CLIs is relatively constant. The proposed faulty line identification, fault type determination, and fault poles identification criteria are always valid. Therefore, the proposed fault detection method can achieve fast and accurate detection of DC faults under different current-limiting inductances.

5.5. Influence of Power Reversal on Proposed Method

The active power of the converters 2 and 3 are set to reverse from 2.5 MW to −2.5 MW at 0.5 s, and the voltage waveforms of the CLIs are shown in Figure 11.

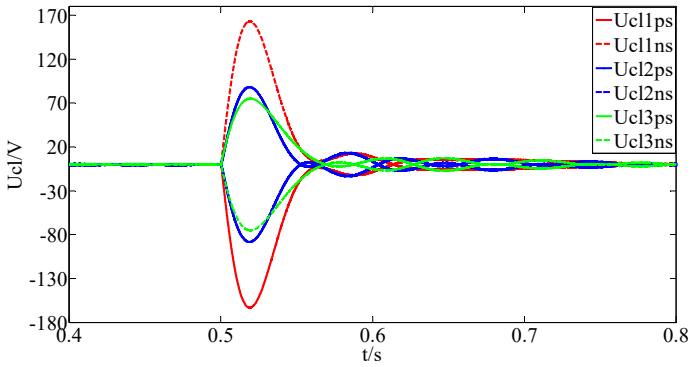

Figure 11. Voltage waveforms of the CLIs with power reversal.

As shown in Figure 11, when the power of the converters 2 and 3 reverse at 0.5 s, the voltages of the CLIs increase rapidly, but the voltage change rates are less than that of the pole-to-pole and pole-to-ground faults. The maximum voltage of the CLIs is only 170 V, which is far below the faulty line identification threshold. Therefore, the power reversal does not affect the proposed fault detection method.

5.6. Influence of AC Fault on Proposed Method

A three-phase fault is applied on the AC side of the converter 1 at 0.5 s. The voltage waveforms of the CLIs are shown in Figure 12.

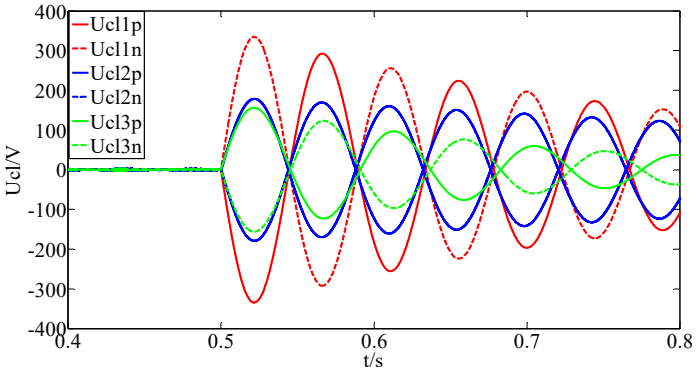

Figure 12. Voltage waveforms of the CLIs during the AC three-phase fault.

As shown in Figure 12, after a three-phase AC fault, the voltages of the CLIs increase rapidly and then attenuate gradually. The maximum amplitude of the voltage of the CLIs is less than 400 V, and the voltage change rates of the CLIs are much lower than that of the DC fault. Therefore, the AC fault does not affect the DC fault detection method proposed in this paper.

5.7. Influence of DC Line Voltage Disturbance on Proposed Method

A DC line voltage disturbance is applied on the DC line of converter 3 at 0.5 s. The voltages of the DC lines and the CLIs are shown in Figure 13.

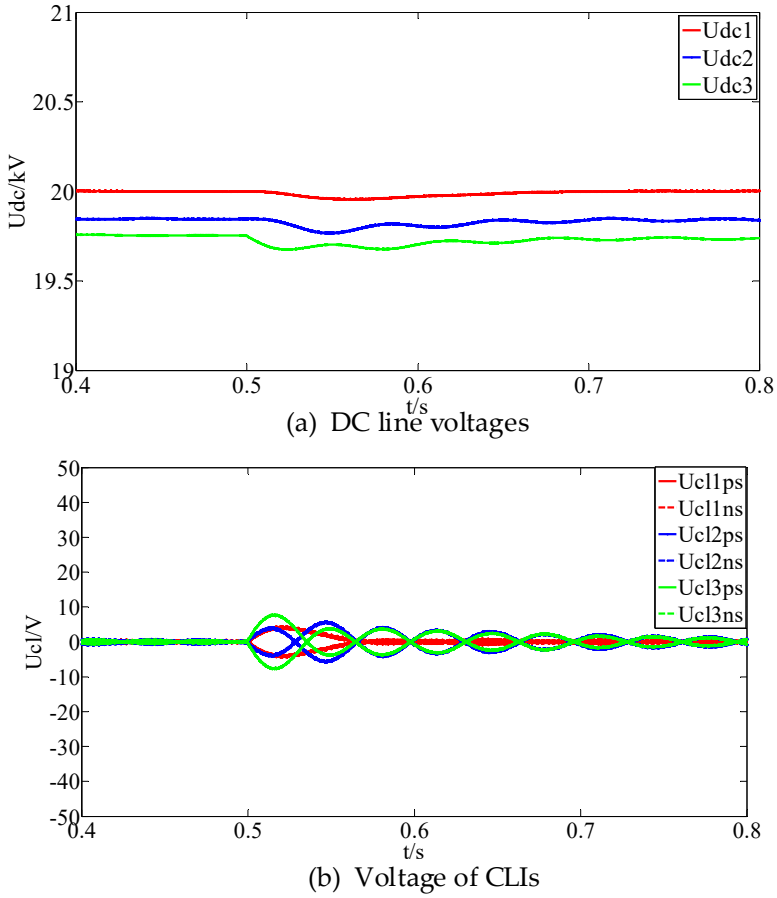

Figure 13. Voltage waveforms of the DC line voltages and the CLIs during the voltage disturbance.

As shown in Figure 13, after a DC line voltage disturbance, the voltages of the DC lines changes and the voltages of the CLIs start to oscillate. However, the disturbance is small and the oscillation amplitudes of the voltages of the CLIs are less than 10 V, which has no influence on the results of the DC fault detection. Therefore, the proposed method keeps unaffected by the DC line voltage disturbance. Furthermore, the time of the DC fault ride-through is much longer than that of the fault detection [29,30]. Therefore, the influence of the voltage regulation and control on the fault detection method can be ignored and is not considered in this paper.

5.8. Fault Detection of Multi-Terminal Ring AC/DC Hybrid Distribution Network

Take the ring AC/DC hybrid distribution network as an example to verify the proposed method. The topology of the three-terminal ring AC-DC hybrid distribution network is shown in Figure 14. The model parameters in Figure 14 are the same as the model shown in Figure 5 except the connection way of the converters.

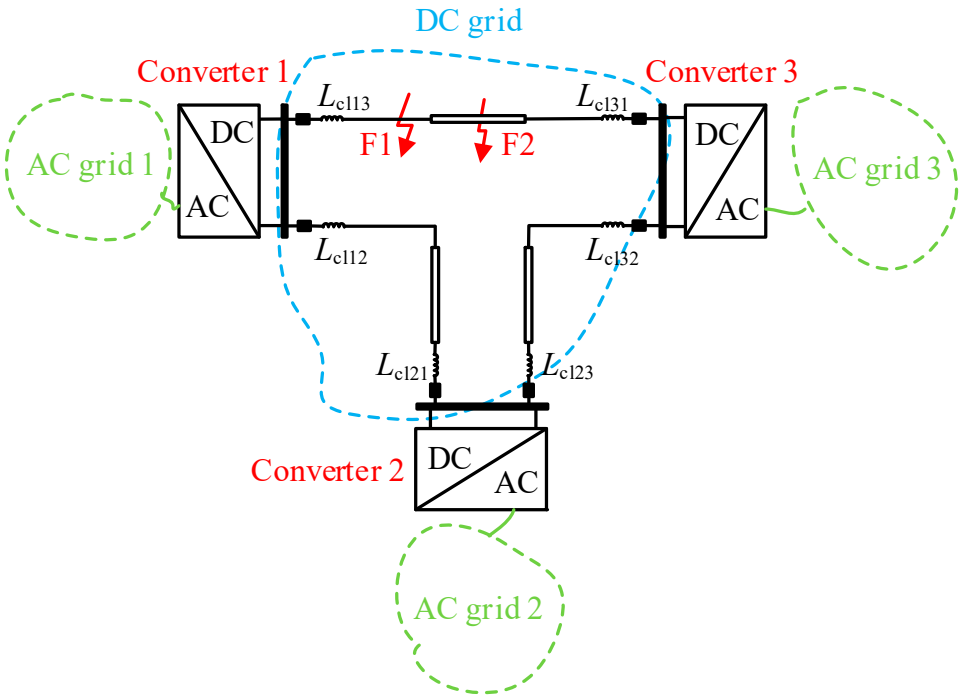

Figure 14. Simulation model of multi-terminal ring AC/DC hybrid distribution network.

5.8.1. Influence of Fault Resistance on Proposed Method

The pole-to-pole fault is applied at 0.5 s at the fault position F1. The currents and voltages of the CLIs after the fault are shown in Figure 15.

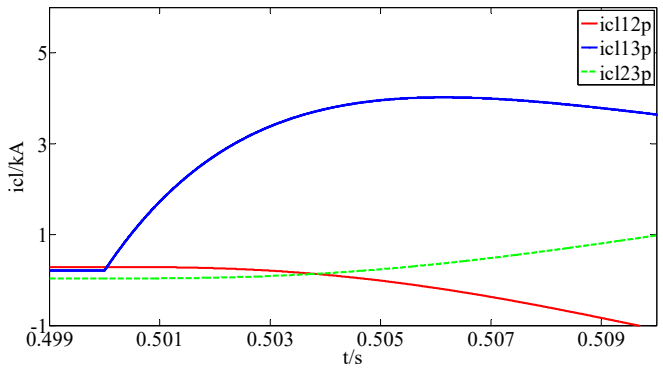

(a) Currents of the CLIs during pole-to-pole fault

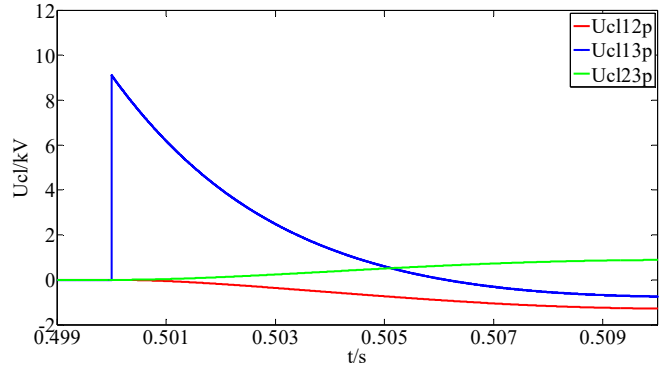

(b) Voltages of the CLIs during pole-to-pole fault

Figure 15. Simulation results of the CLI currents and voltages during DC line 13 pole-to-pole fault.

As shown in Figure 15, after the pole-to-pole fault on the DC line 13, the currents and voltages of the CLIs increase rapidly and then attenuate gradually, which is similar to the case in the radial network. There is an evident difference in the voltage change rates between the CLIs on the faulty line and non-faulty lines. Therefore, the proposed fault detection method can be used in this system.

The pole-to-pole fault and pole-to-ground fault are applied at 0.5 s at fault positions F1 and F2. In addition, the fault resistance varies from 0 Ω to 80 Ω. The voltage change rates of the CLIs are shown in Figure 16.

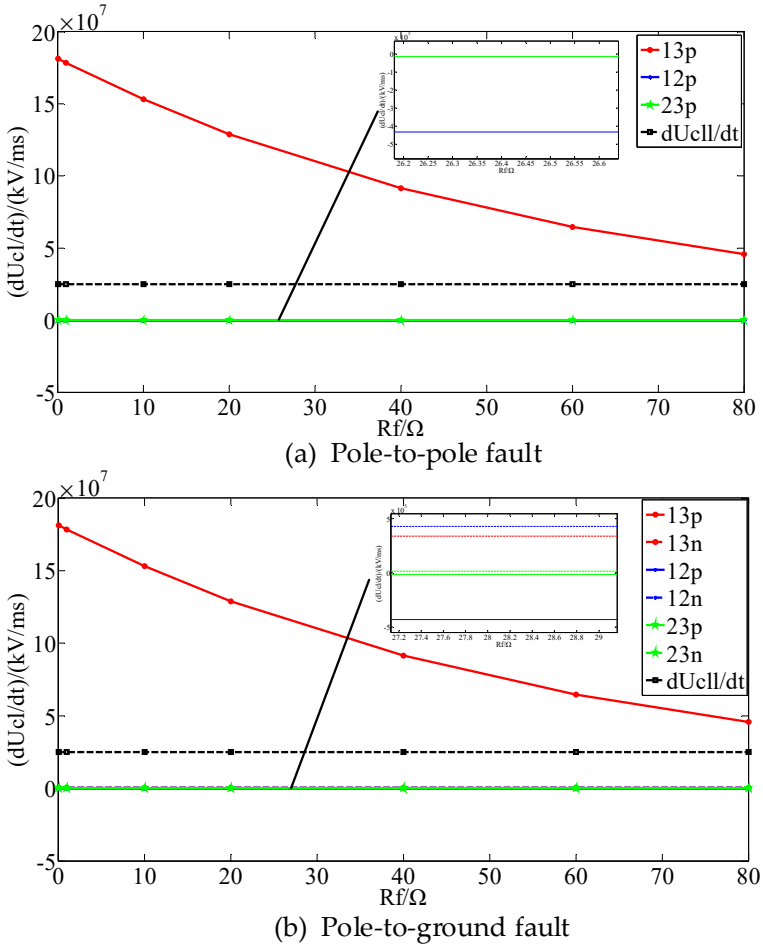

Figure 16. Voltage change rates of the CLIs during DC faults with different fault resistances.

As shown in Figure 16, for the pole-to-pole fault, the voltage change rates of the CLIs on the faulty line decrease as the increase of the fault resistance, and the voltage change rates of the CLIs on the non-faulty lines keep almost unchanged. The voltage change rates of the CLIs on the faulty lines are always greater than that of the non-faulty lines and the proposed fault detection method is always feasible. For the pole-to-ground fault, the influence of the fault resistance on the voltage change rates of the CLIs is similar to that of the pole-to-pole fault. The proposed fault detection method can detect the pole-go-ground fault accurately. Therefore, in the ring AC-DC hybrid distribution network, the proposed fault detection method is also feasible and is not affected by the fault resistance.

5.8.2. Influence of Power Reversal on Proposed Method

The active power of the converters 2 and 3 are set to reverse from 2.5 MW to −2.5 MW at 0.5 s, the voltage waveforms of the CLIs are shown in Figure 17.

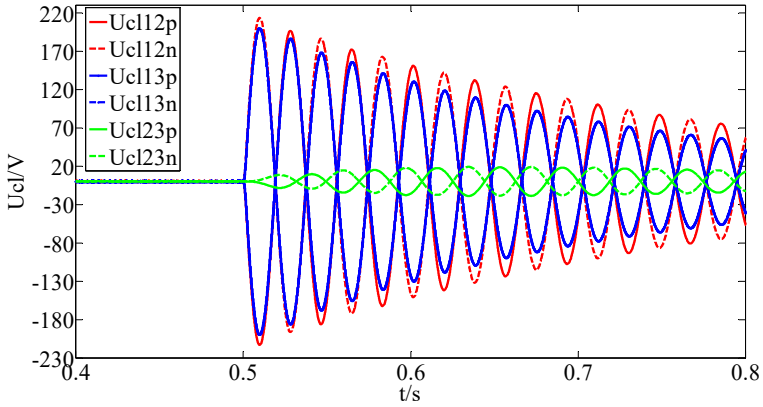

Figure 17. Voltage waveforms of the CLIs with power reversal.

As shown in Figure 17, when the power of the converter stations 2 and 3 reverse at 0.5 s, the voltages of the CLIs will increase, but the maximum value of them is about 220 V, which is much lower than that of the DC faults. Therefore, the power reversal does not affect the proposed fault detection method in the ring AC/DC hybrid distribution network.

In conclusion, the proposed fault detection method can achieve DC fault detection of multi-terminal AC/DC hybrid distribution network under various fault conditions, including different fault resistances, different fault locations, different current-limiting inductances and power reversal of converters. The primary fault detection method and backup fault detection method can detect all DC faults with different resistances and will not be triggered falsely by the AC faults.

6. Conclusions

This paper analyzes the voltage and current characteristics of the CLIs in the AC/DC hybrid distribution network and concludes that the voltages of the CLIs increase rapidly after the DC line faults and then attenuate gradually. The proposed fault detection method based on the voltage change rate of the CLI can detect low-resistance and high-resistance faults quickly and accurately. For the low-resistance fault, the voltage change rates of the single-ended CLIs are used to detect the faulty line, fault type and fault poles. For the high-resistance fault, the voltage change rates of the CLIs on two ends of the DC lines are used to identify the faulty line. Then the voltage change rate of the CLI on one end of the faulty line is used to determine the fault type and fault poles. The fault detection criteria are simple and easy to be achieved. In addition, the DC faults can be detected within 2 ms. The simulation results show that the proposed method is not affected by the fault location and the DC pole-to-pole fault and pole-to-ground fault can be detected accurately under different fault locations. The inductances of the CLIs, the power reversal and the DC line voltage disturbance have little influence on the voltage change rates of the CLIs and the proposed method is feasible under these conditions. The AC fault can lead to the oscillation of the voltage change rates of the CLIs, while the influence is too little to affect the fault detection results. When the fault resistance varies, the primary detection method and the back-up detection method can work together and detect all kinds of DC faults quickly and accurately. In addition, the proposed method is also suitable for multi-terminal AC/DC hybrid distribution networks with different topologies such as radial topology, ring topology and so on.

In summary, the proposed DC fault detection method for the AC/DC hybrid distribution network bases on the voltage change rates of the CLIs, which is easy to sample and calculate. The detection of the DC faults can be completed within 2 ms. In addition, the fault characteristics used by the proposed method is accurate enough to determine the faulty line, fault type and fault poles. The primary detection method satisfies the requirement of the detection time and the back-up detection method uses the signals from two ends of the faulty line, which needs more detection time than the primary

detection method but is not affected by the change of fault resistances. All kinds of DC faults can be detected accurately using the proposed method and the accuracy is up to 100%. This leads to the fast and accurate operation of the protection devices and is beneficial to the isolation of DC faults. Furthermore, the proposed method is feasible to any DC faults that have a DC capacitor discharge stage. The proposed method has high reliability, low cost and high robustness, which indicates a promising application in the multi-terminal AC/DC hybrid distribution network. In future, the proposed method will be applied in the model built by the RT-LAB and its feasibility will be verified further in subsequent publications.

Author Contributions: Conceptualization, X.Q.; Methodology, X.Q.; Software, X.Q. and L.L.; Validation, X.Q.; Formal Analysis, X.Q.; Investigation, X.Q.; Resources, X.Q. and L.K.; Data Curation, X.Q.; Writing-Original Draft Preparation, X.Q.; Writing-Review & Editing, X.Q., W.P. and L.K.; Visualization, X.Q., W.P. and L.K.; Supervision, W.P. and L.K.; Project Administration, W.P. and L.K.; Funding Acquisition, W.P., and L.K.

Funding: This research was funded by the National Key Research and Development Program of China (2017YFB0903300) and the Key Front Science Project of Chinese Academy of Sciences (QYZDY-SSW-JSC025).

Conflicts of Interest: The authors declare no conflict of interest.

References

1. Boroyevich, D.; Cvetković, I.; Dong, D.; Burgos, R.; Wang, F.; Lee, F. Future Electronic Power Distribution Systems: A Contemplative View. In Proceedings of the 12th International Conference on Optimization of Electrical and Electronic Equipment, Basov, Romania, 20–22 May 2010; pp. 1369–1380.
2. Jamali, S.Z.; Bukhari, S.B.A.; Khan, M.O.; Mehdi, M.; Noh, C.-H.; Gwon, G.-H.; Kim, C.-H. Protection Scheme of a Last Mile Active LVDC Distribution Network with Reclosing Option. *Energies* **2018**, *11*, 1093. [CrossRef]
3. Guillod, T.; Krismer, F.; Kolar, J.W. Protection of MV Converters in the Grid: The Case of MV/LV Solid-State Transformers. *IEEE J. Emerg. Sel. Top. Power Electron.* **2017**, *5*, 393–408. [CrossRef]
4. Bucher, M.K.; Franck, C.M. Analytic Approximation of Fault Current Contributions from Capacitive Components in HVDC Cable Networks. *IEEE Trans. Power Deliv.* **2015**, *30*, 74–81. [CrossRef]
5. Li, C.; Zhao, C.; Xu, J.; Ji, Y.; Zhang, F.; An, T. A Pole-to-Pole Short-Circuit Fault Current Calculation Method for DC Grids. *IEEE Trans. Power Syst.* **2017**, *32*, 4943–4953. [CrossRef]
6. Park, J.-D.; Candelaria, J. Fault Detection and Isolation in Low-Voltage DC-Bus Micro-grid System. *IEEE Trans. Power Deliv.* **2013**, *28*, 779–787. [CrossRef]
7. Fletcher, S.D.A.; Norman, P.J.; Fong, K.; Galloway, S.J.; Burt, G.M. High-Speed Differential Protection for Smart DC Distribution Systems. *IEEE Trans. Smart Grid.* **2014**, *5*, 2610–2617. [CrossRef]
8. Meghwani, A.; Srivastava, S.C.; Chakrabarti, S. A Non-Unit Protection Scheme for DC Micro-grid Based on Local Measurements. *IEEE Trans. Power Deliv.* **2017**, *32*, 172–181. [CrossRef]
9. Sneath, J.; Rajapakse, A.D. Fault Detection and Interruption in an Earthed HVDC Grid Using ROCOV and Hybrid DC Breakers. *IEEE Trans. Power Deliv.* **2016**, *31*, 973–981. [CrossRef]
10. Li, R.; Xu, L.; Yao, L. DC Fault Detection and Location in Meshed Multi-terminal HVDC Systems Based on DC Reactor Voltage Change Rate. *IEEE Trans. Power Deliv.* **2017**, *32*, 1516–1526. [CrossRef]
11. Li, J.; Tai, N.; Fan, C. Transient-Voltage Based Protection Scheme for DC Line Faults in Multi-Terminal VSC-HVDC System. *IEEE Trans. Power Deliv.* **2017**, *32*, 1483–1494. [CrossRef]
12. Liu, J.; Tai, N.; Fan, C.; Yang, Y. Transient Measured Impedance-Based Protection Scheme for DC Line Faults in Ultra High-Voltage Direct-Current System. *IET Gener. Transm. Distrib.* **2016**, *10*, 3597–3609. [CrossRef]
13. Haleem, N.M.; Rajapakse, A.D. Application of New Directional Logic to Improve DC Side Fault Discrimination for High Resistance Faults in HVDC Grids. *J. Mod. Power Syst. Clean Energy* **2017**, *5*, 560–573. [CrossRef]
14. Saleh, K.A.; Hooshyar, A.; El-Saadany, E.F. Hybrid Passive-Overcurrent Relay for Detection of Faults in Low-Voltage DC grids. *IEEE Trans. Smart Grid.* **2017**, *8*, 1129–1138. [CrossRef]
15. Liu, G.; Xu, F.; Xu, Z.; Zhang, Z.; Tang, G. Assembly HVDC Breaker for HVDC grids With Modular Multilevel Converters. *IEEE Trans. Power Electron.* **2017**, *32*, 931–941. [CrossRef]
16. Xu, Z.; Xiao, H.; Xiao, L.; Zhang, Z. DC Fault Analysis and Clearance Solutions of MMC-HVDC Systems. *Energies* **2018**, *11*, 941. [CrossRef]

17. Tang, L.; Ooi, B.-T. Locating and Isolating DC Faults in Multi-Terminal DC Systems. *IEEE Trans. Power Deliv.* **2007**, *22*, 1877–1884. [CrossRef]
18. Monadi, M.; Koch-Ciobotaru, C.; Luna, A.; Candela, J.I.; Rodriguez, P. Multi-Terminal Medium Voltage DC Grids Fault Location and Isolation. *IET Gener. Transm. Distrib.* **2016**, *10*, 3517–3528. [CrossRef]
19. Tzelepis, D.; Dysko, A.; Fusiek, G.; Nelson, J.; Niewczas, P.; Vozikis, D.; Orr, P.; Gordon, N.; Booth, C.D. Single-Ended Differential Protection in MTDC Networks Using Optical Sensors. *IEEE Trans. Power Deliv.* **2017**, *32*, 1605–1615. [CrossRef]
20. Lewis, P.T.; Grainger, B.M.; AI Hassan, H.A.; Barchowsky, A.; Reed, G.F. Fault Section Identification Protection Algorithm for Modular Converter-Based High Voltage DC with a Hybrid Transmission Corridor. *IEEE Trans. Ind. Electron.* **2016**, *63*, 5652–5662. [CrossRef]
21. Leterme, W.; Beerten, J.; Hertem, D.V. Nonunit Protection of HVDC Grids with Inductive DC Cable Termination. *IEEE Trans. Power Deliv.* **2016**, *31*, 820–828. [CrossRef]
22. Salomonsson, D.; Söder, L.; Sannino, A. Protection of Low-Voltage DC Microgrids. *IEEE Trans. Power Deliv.* **2009**, *24*, 1045–1053. [CrossRef]
23. Baran, M.E.; Mahajan, N.R. Overcurrent Protection on Voltage-Source-Converter-Based Multiterminal DC Distribution Systems. *IEEE Trans. Power Deliv.* **2007**, *22*, 406–412. [CrossRef]
24. Fletcher, S.D.A.; Norman, P.J.; Galloway, S.J.; Crolla, P.; Burt, G.M. Optimizing the Roles of Unit and Non-unit Protection Methods Within DC Microgrids. *IEEE Trans. Smart Grid.* **2012**, *3*, 2079–2087. [CrossRef]
25. Nuutinen, P.; Peltoniemi, P.; Silventoinen, P. Short-Circuit Protection in a Converter-Fed Low-Voltage Distribution Network. *IEEE Trans. Power Electron.* **2013**, *28*, 1587–1597. [CrossRef]
26. Hernandez, J.C.; Sutil, F.S.; Vidal, P.G. Protection of a Multiterminal DC Compact Node Feeding Electric Vehicles on Electric Railway Systems, Secondary Distribution Networks, and PV Systems. *Turk. J. Electr. Eng. Comput. Sci.* **2016**, *24*, 3123–3143. [CrossRef]
27. Yang, J.; Fletcher, J.E.; O'Reilly, J. Short-Circuit and Ground Fault Analyses and Location in VSC-Based DC Network Cables. *IEEE Trans. Ind. Electron.* **2012**, *59*, 3827–3837. [CrossRef]
28. Belda, N.A.; Plet, C.A.; Smeets, R.P.P. Analysis of Faults in Multiterminal HVDC Grid for Definition of Test Requirements of HVDC Circuit Breakers. *IEEE Trans. Power Deliv.* **2018**, *33*, 403–411. [CrossRef]
29. Li, R.; Yao, L.; Williams, B.W. Active Control of DC Fault Currents in DC Solid-State Transformers During Ride-Through Operation of Multi-Terminal HVDC Systems. *IEEE Trans. Energy Convers.* **2016**, *31*, 1336–1346. [CrossRef]
30. Sanusi, W.; Hosani, M.A.; Moursi, M.S.E. A Novel DC Fault Ride-Through Scheme for MTDC Networks Connecting Large-Scale Wind Parks. *IEEE Trans. Sustain. Energy* **2017**, *8*, 1086–1095. [CrossRef]

© 2018 by the authors. Licensee MDPI, Basel, Switzerland. This article is an open access article distributed under the terms and conditions of the Creative Commons Attribution (CC BY) license (http://creativecommons.org/licenses/by/4.0/).